NISTIR 6545

Analysis of CCRL Proficiency Cements 135 and 136 Using CEMHYD3D

Dale P. Bentz
Xiuping Feng
Claus-Jochen Haecker
Paul E. Stutzman

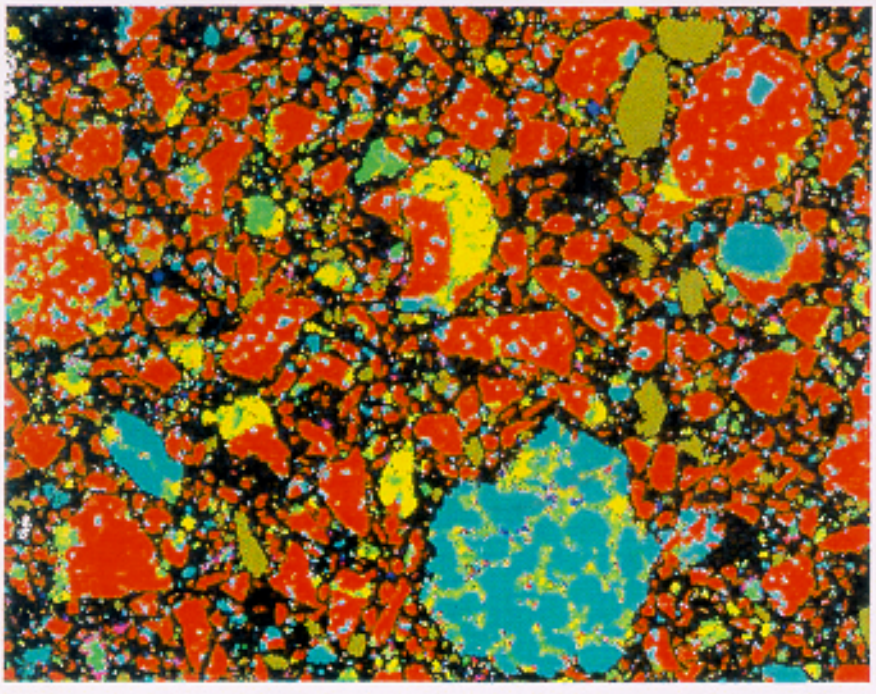

1901-2001
NIST CENTENNIAL

NIST

National Institute of Standards and Technology
Technology Administration, U.S. Department of Commerce

NISTIR 6545

Analysis of CCRL Proficiency Cements 135 and 136 Using CEMHYD3D

Dale P. Bentz
Xiuping Feng
Claus-Jochen Haecker
Paul E. Stutzman
Building and Fire Research Laboratory

August 2000

U.S. Department of Commerce
Norman Y. Mineta, Secretary

Technology Administration
Dr. Cheryl L. Shavers, Under Secretary of Commerce for Technology

National Institute of Standards and Technology
Raymond G. Kammer, Director

ABSTRACT

This NISTIR provides experimental and computer modeling results for cements 135 and 136 issued by the Cement and Concrete Reference Laboratory at NIST in January of 2000. The purposes of this report are to characterize these cements via scanning electron microscopy (SEM) analysis and to document the ability of the NIST computer model, CEMHYD3D, to predict the hydration kinetics, heat of hydration, and mortar strength development of Portland cements evaluated in the CCRL proficiency sample program. The general procedure to evaluate a new cement is as follows: 1) two-dimensional SEM backscattered electron and X-ray microanalysis images of the cement of interest are obtained, along with a measured particle size distribution (PSD), 2) based on analysis of these images and the measured PSD, three-dimensional microstructures of various water-to-cement ratios are created and hydrated using CEMHYD3D, and 3) the model predictions for degree of hydration under saturated and sealed conditions, heat of hydration (ASTM C186), and strength development of mortar cubes (ASTM C109) are compared to experimental measurements either performed at NIST or at the participating CCRL proficiency sample evaluation laboratories. For both cements, generally good agreement is observed between the model predictions and the experimental data, demonstrating the predictive capabilities of CEMHYD3D.

Keywords: Building technology, computer modeling, cement, heat of hydration, hydration kinetics, particle size distribution, SEM imaging, strength development.

Contents

List of Figures

List of Tables

1 Introduction

Twice each year, the Cement and Concrete Reference Laboratory (CCRL), housed at the National Institute of Standards and Technology (NIST), issues two proficiency samples of portland cement to be evaluated by hundreds of testing laboratories throughout the United States using ASTM standard test methods [1]. The chemical characteristics and performance properties of these cements are therefore extremely well documented [2], making them ideal systems to study with the NIST cement hydration and microstructural development computer model (CEMHYD3D) [3, 4]. In this report, scanning electron microscopy (SEM) images and quantitative phase analysis results for cements 135 and 136, issued in January of 2000, will be presented and compared to the potential phase composition determined via ASTM C150 [1]. Additionally, CEMHYD3D and supplemental experimental measurements will be applied to predicting the hydration kinetics, heat of hydration, and mortar strength development of the two cements. The latter two properties can be compared to those measured as part of the CCRL proficiency sample analysis program.

2 Experimental Procedure

Proficiency samples of CCRL cements 135 and 136 were obtained in January of 2000. The samples were provided double-sealed in plastic bags in cardboard boxes. Samples of the two cement powders were subsequently analyzed with respect to particle size distribution and by scanning electron microscopy and X-ray microanalysis.

2.1 Particle Size Distribution

The particle size distributions of CCRL cements 135 and 136 were determined using laser diffraction techniques at the laboratories of Dyckerhoff Zement in Germany. For the measurements, a HELOS instrument type RODOS T4.1 from SYMPATEC GmbH, Germany[1] was used .

For the measurements, a 100 g sample of each cement was divided into 10 equal subsamples, each of which was evaluated separately. The focal distance of the HELOS instrument was set at 87.5 μm, allowing the measurement of particles with diameters between 0.25 μm and 87.5 μm. The sample feeding was adjusted in such a way that the so-called "optical" concentration of the cement particles in the measuring cell ranged from 7.5 % to 14.6 % for cement 135 and from 5.6 % to 14.1 % for cement 136. The measuring time varied between 10 s and 30 s per subsample. The average PSD curves computed by averaging the results obtained for the 10 subsamples of each cement are shown in Figure 1. The PSDs measured for the two cements are seen to be quite similar, as are their Blaine finenesses (cement 135: 394 m^2/kg and cement 136: 390 m^2/kg) measured via the standard ASTM C204 technique [1] in the CCRL testing program [2].

[1] Certain commmercial equipment is identified in this report to specify the experimental procedure. In no case does such identification imply endorsement by the National Institute of Standards and Technology, nor does it indicate that the equipment is necessarily the best available for the purpose.

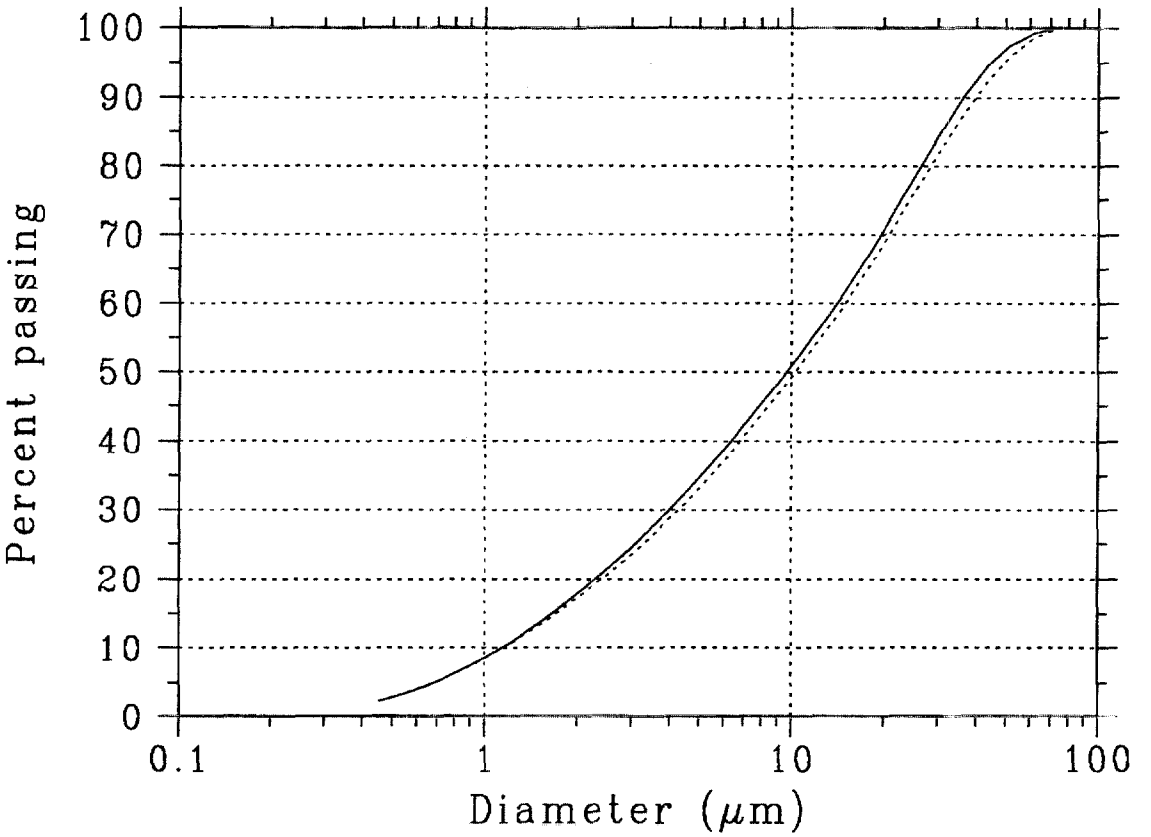

Figure 1: Measured cement particle size distributions for CCRL cements 135 (solid line) and 136 (dotted line). Curves shown are the mean values of ten separate measurements.

2.2 Scanning Electron Microscopy Imaging

The sample preparation techniques for samples to be analyzed using SEM have been described in detail elsewhere [5, 6], but will be briefly reviewed here. To prepare a polished specimen for viewing in the SEM, approximately 25 g of the powder to be imaged is blended with an epoxy resin to form an extremely viscous paste. The resin/powder mixture is pressed into a small cylindrical mold and cured at 60 °C for 24 h. The cured specimen is then cut to obtain a plane surface for imaging.

Saw marks are removed by grinding with 400 grit followed by 600 grit sandpaper. Final polishing is done on a lap wheel with (6, 3, 1, and 0.25) μm diamond paste for 30 s each. After each polishing, the specimen is cleaned using a clean cloth. After the final polishing step, ethanol is used to remove any residual polishing compound. The final polished specimen is coated with carbon to provide a conductive surface for viewing in the SEM.

Once properly prepared, the specimen is placed in the SEM viewing chamber, and signals are collected for the backscattered electrons and X-rays. Typical accelerating voltage and probe current for the backscattered electron images are 12 kV and 2 nA, respectively. For the X-ray images, the probe current is increased to about 10 nA. For analysis of cement powders, in addition to the backscattered electron signal, X-ray images are collected for Ca, Si, Al, Fe, S, K, and Mg. Because these X-ray images are collected at the same location as the backscattered electron image, this series of images can be combined to determine the mineral phase present at each location (pixel) in the two-dimensional image (typically 512

pixels by 400 pixels in size). Typically, magnifications of 250X or 500X are employed for obtaining the SEM and X-ray images. Examples of composite X-ray images for cements 135 and 136 are shown in Figures 3 and 5, respectively. In these images, three different X-ray signal intensities (Ca, Si, and Al) have been mapped into the three color signal channels (red, green, and blue), respectively.

To process the input SEM/X-ray images and to determine the distribution of phases, a decision tree is traversed for each pixel location in the images. An example of a decision tree for a typical cement powder is shown in Figure 2. In this figure, X^* represents a critical threshold greylevel value. Pixels having a greylevel greater than the value of X^* are considered to contain the element of interest and those with a greylevel below X^* are classified as not containing the element. To determine the values of X^* for each element, the corresponding greylevel histogram [7] for each X-ray image is viewed.

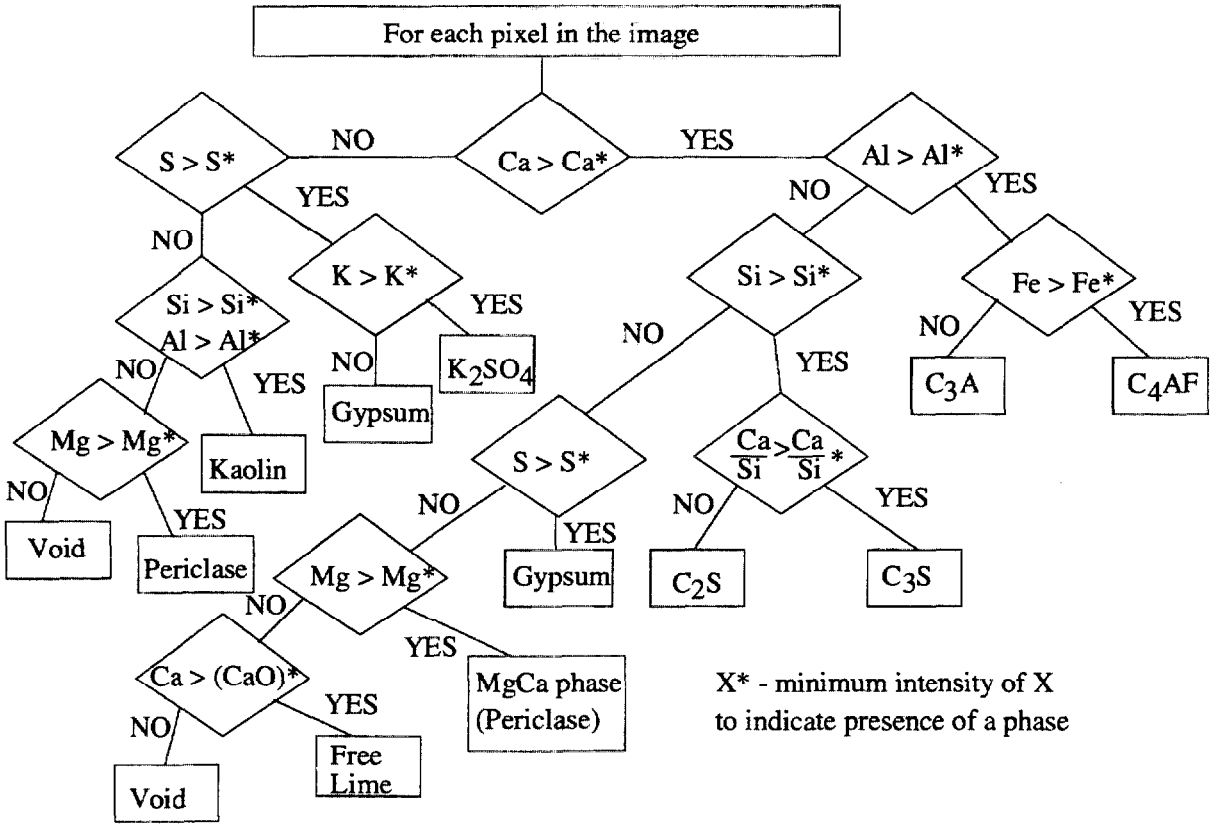

Figure 2: Segmentation algorithm for separating portland cement into its components. C_3S denotes tricalcium silicate, C_2S denotes dicalcium silicate, C_3A denotes tricalcium aluminate, C_4AF denotes tetracalcium aluminoferrite, and CaO corresponds to free lime.

After the segmentation tree is traversed, the segmented image produced will still contain a substantial amount of random noise. To improve the image quality, three "filters" are applied in succession to the processed image. First, all isolated one pixel "solid" pixels are converted to porosity. Second, all isolated one pixel "pores" (totally surrounded by solids) are converted to the majority surrounding solid phase. Finally, a median filter [7] is applied to replace each solid pixel by the majority solid phase present in the surrounding neighborhood,

typically a centered 5 pixel × 5 pixel square. This three-fold process removes the remaining noise present in the segmented image, producing an image ready for quantitative stereological analysis, such as those shown in Figures 4 and 6 for cements 135 and 136, respectively. For both cements 135 and 136, two separate image composites were acquired and processed in this manner. These and images for a variety of other cements are available in a prototype online cement images database, being developed within the NIST Partnership for High Performance Concrete Technology program. The prototype database is available for viewing over the Internet at http://ciks.cbt.nist.gov/phpct/database/images.

2.3 Mathematical Analysis of Cement Images

The final processed images can be analyzed to determine any number of stereological parameters. For cement hydration, parameters of interest include phase area fractions and phase surface perimeter fractions. For an isotropic system, the area fraction of a phase present in a 2-D image will directly correspond to its volume fraction in three dimensions. Similarly, a phase's share of the total perimeter (solid pixels in contact with porosity) will correspond to its share of the total surface area in 3-D. The surface area fractions of the phases are particularly important for cement hydration as the hydration reactions with water occur at the surfaces of the particles. Examples of the quantitative analyses determined using this evaluation procedure are provided in Figures 7 and 8 for cements 135 and 136, respectively. These results are also available in the cement images database at http://ciks.cbt.nist.gov/phpct/database/images.

For an isotropic material, the spatial correlation functions are identical in two and three dimensions, simply being a function of distance, r. Thus, the measured 2-D correlation function for a phase or a combination of phases can be used to reconstruct a 3-D representation of the cement particles [3]. For an $M \times N$ image, the two-point correlation function for a phase, $S(x, y)$, is determined as:

$$S(x,y) = \sum_{i=1}^{M-x} \sum_{j=1}^{N-y} \frac{I(i,j) \times I(i+x, y+j)}{(M-x) \times (N-y)} \tag{1}$$

where I(x,y) is one if the pixel at location (x,y) contains the phase(s) of interest and 0 otherwise. S(x,y) is easily converted to S($r = \sqrt{x^2 + y^2}$) for distances r in pixels. Because the correlation function implicitly contains information on the volume fraction and specific surface of the phase(s) being analyzed, this function can be employed to reconstruct a three-dimensional representation of the cementitious particles that matches the phase volume and surface area fractions and correlation structure of the 2-D final SEM image. These starting 3-D structures of cement particles in water can then be used as input images for the CEMHYD3D cement hydration and microstructure development computer model [3, 4].

The phase compositions estimated using the SEM and image analysis are compared to those calculated based on the cement oxide composition using ASTM C150 [1] in Tables 1 and 2. For both cements 135 and 136, the SEM-measured values for C_3S significantly exceed those calculated using ASTM C150, while the values for C_2S and C_3A are generally less than those calculated from the oxide compositions. The calculations presented in ASTM C150 are known to be only approximate [8], with quantitative optical point counting (ASTM C1356M) [1] or X-ray diffraction (ASTM C1365) [1] being preferred methods for performing quantitative phase analysis.

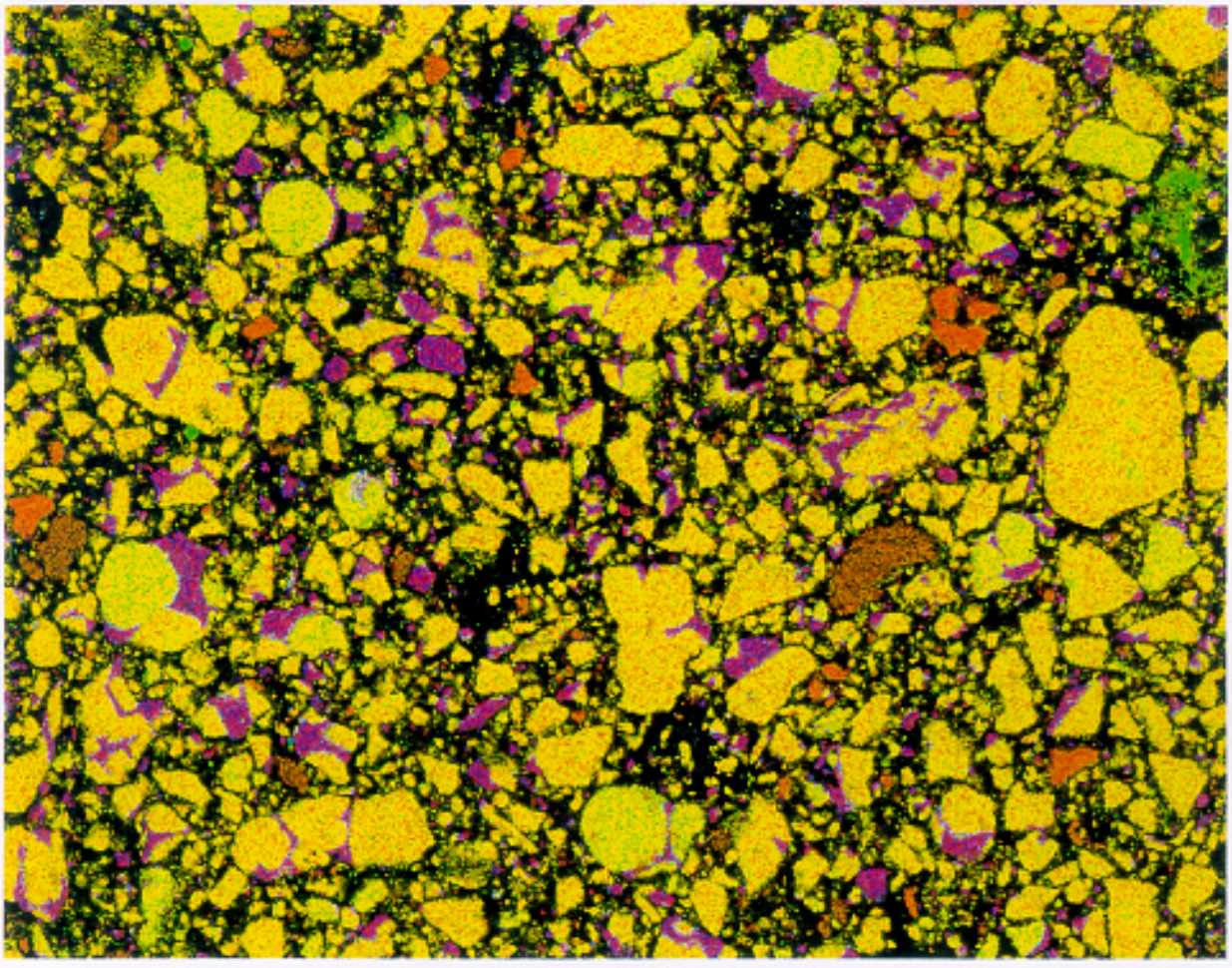

Figure 3: Composite RGB image of cement 135. In the composite color image, the degree of red is proportional to the Ca X-ray signal, green the Si, and blue the Al. Thus, shades of yellow would correspond to (red/green or calcium/silicon) calcium silicate phases and shades of purple would correspond to (red/blue or calcium/aluminum) calcium aluminate phases. Black is the epoxy-filled pore space. Image is 256 μm $\times$ 200 μm.

Table 1: Potential Volumetric Phase Compositions for Cement 135

Phase	ASTM C150 composition	SEM analysis composition
C_3S	61.76	67.94 $\pm$ 3.88 [a]
C_2S	21.48	17.14 $\pm$ 3.99
C_3A	7.81	7.03 $\pm$ 0.32
C_4AF	8.95	7.89 $\pm$ 0.42

[a] Indicates standard deviation between the values determined for the two images.

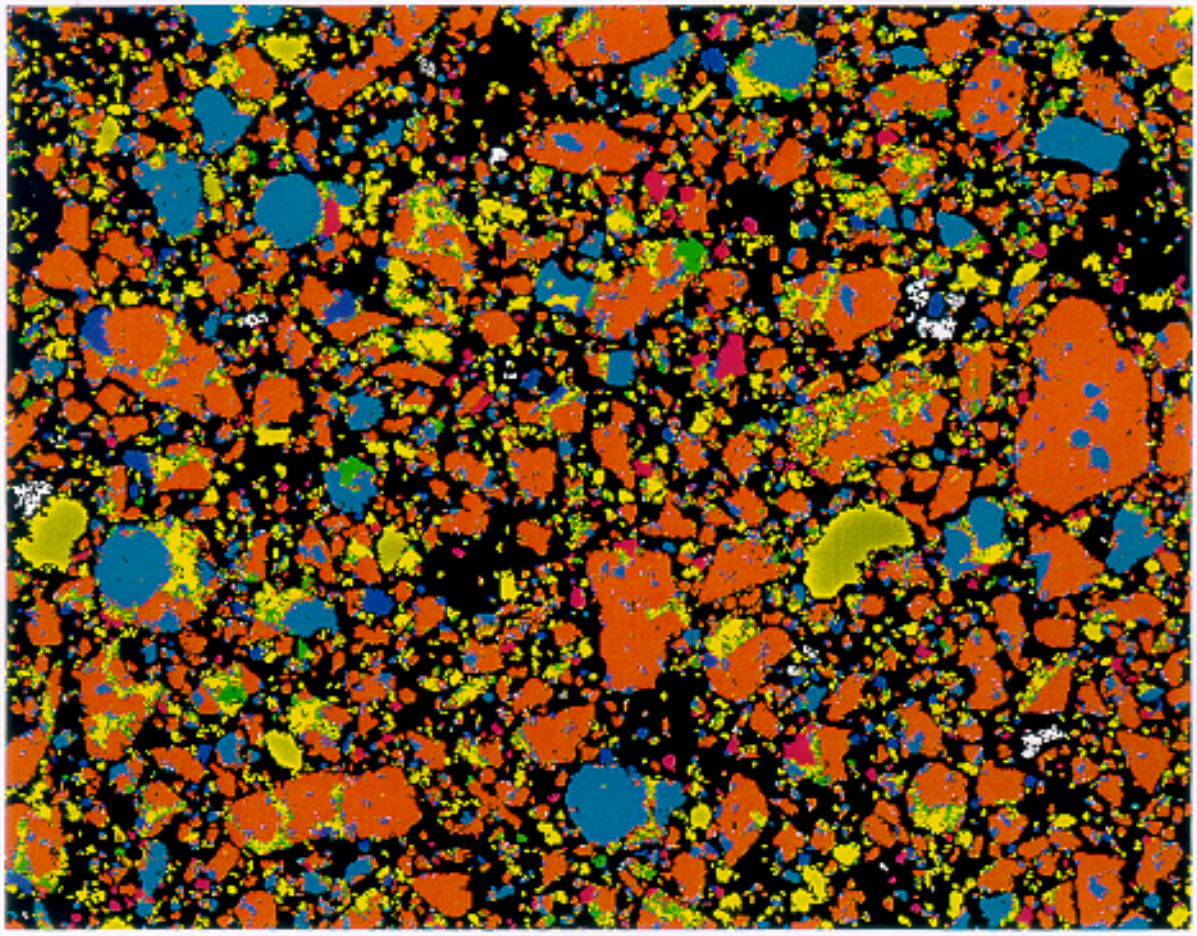

Figure 4: Processed image of cement 135. Red is C_3S, aqua is C_2S, green is C_3A, yellow is C_4AF, pale green is gypsum, white is free lime (CaO), dark blue is K_2SO_4, and magenta is periclase. Image is 256 μm $\times$ 200 μm.

Table 2: Potential Volumetric Phase Compositions for Cement 136

Phase	ASTM C150 composition	SEM analysis composition
C_3S	59.56	65.6 $\pm$ 5.09
C_2S	20.64	18.12 $\pm$ 5.21
C_3A	9.46	6.65 $\pm$ 0.87
C_4AF	10.34	9.63 $\pm$ 0.97

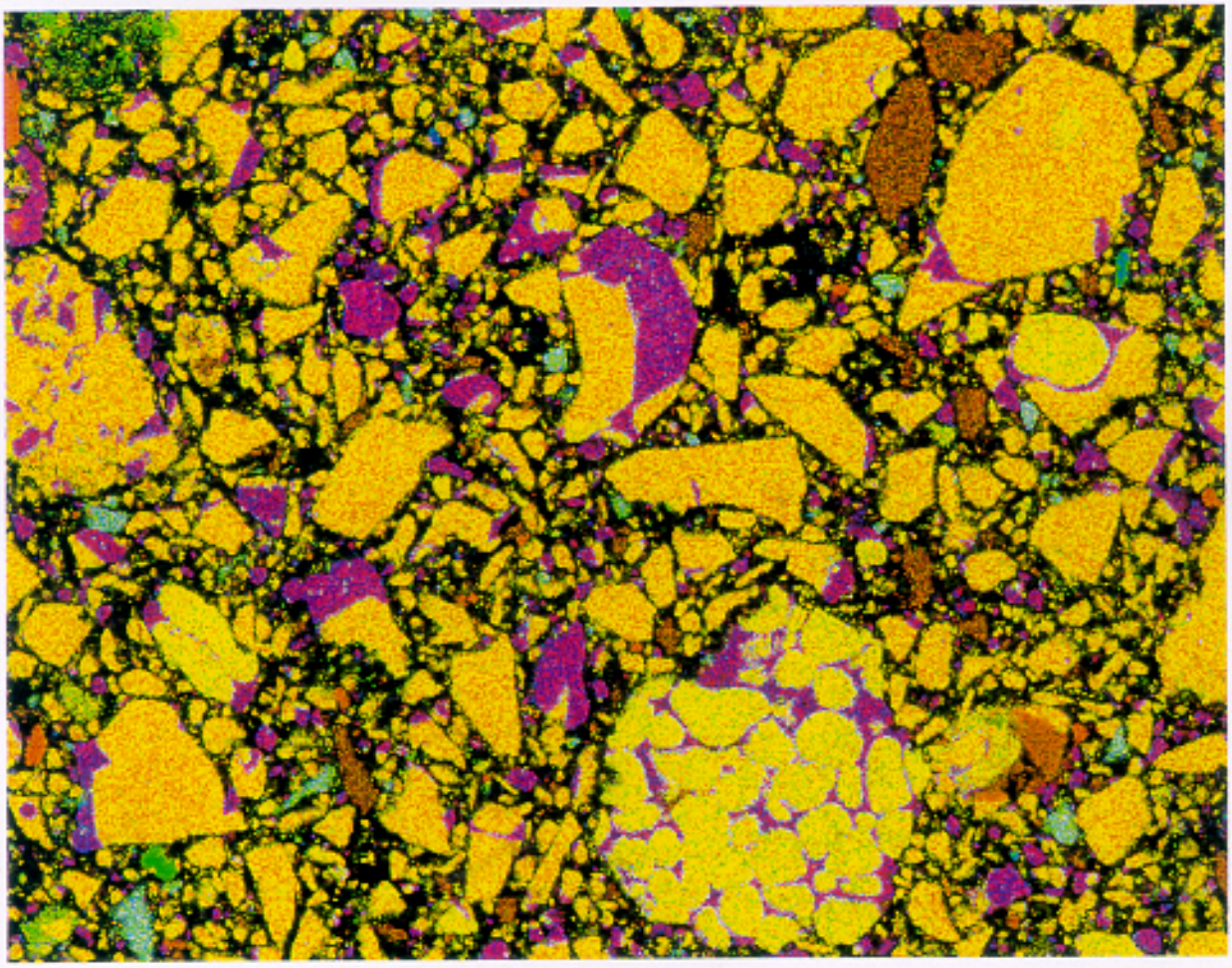

Figure 5: Composite RGB image of cement 136. In the composite color image, the degree of red is proportional to the Ca X-ray signal, green the Si, and blue the Al. Thus, shades of yellow would correspond to (red/green or calcium/silicon) calcium silicate phases and shades of purple would correspond to (red/blue or calcium/aluminum) calcium aluminate phases. Black is the epoxy-filled pore space. Image is 256 μm $\times$ 200 μm.

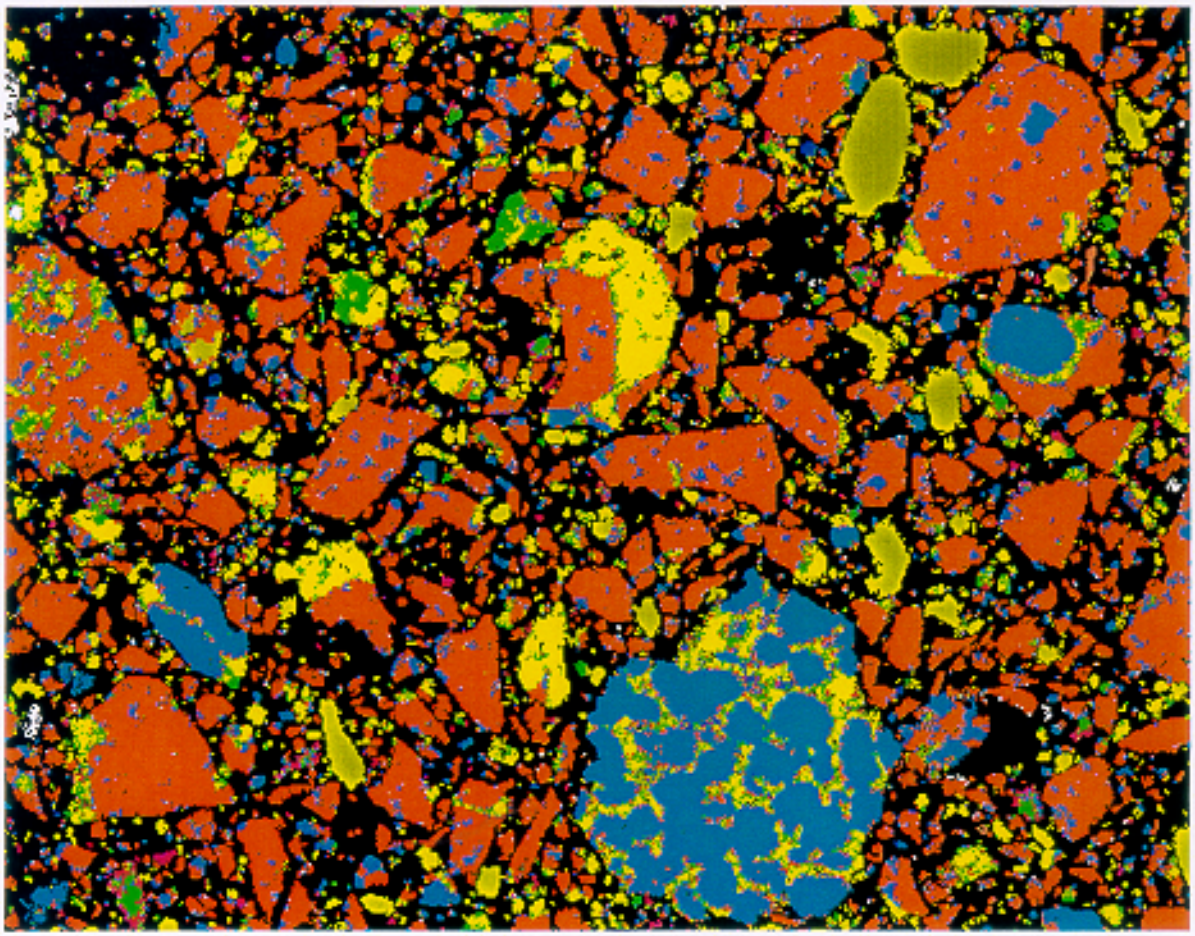

Figure 6: Processed image of cement 136. Red is C_3S, aqua is C_2S, green is C_3A, yellow is C_4AF, pale green is gypsum, white is free lime (CaO), dark blue is K_2SO_4, and magenta is periclase. Image is 256 μm $\times$ 200 μm.

Information on CCRL Cement 135

Image and correlation files for:
Cement and Concrete Reference Laboratory (CCRL) Cement 135, a Type I ordinary portland cement with a Blaine fineness of about 394 m^2/kg

Color 2D image in cement135.gif (500X magnification- 256 μm by 200 μm)
Red is C_3S, aqua is C_2S, green is C_3A, yellow is C_4AF, pale green is gypsum, white is free lime, dark blue is potassium sulfate, and magenta is a MgCa phase

Discretized particle size distribution is in cement135.psd

Extracted Correlation files (1 μm/pixel):
cm135r.sil --- C_3S and C_2S
cm135r.c3s --- C_3S
cm135r.c4f --- C_4AF

Phase Fractions for four major clinker phases (average of two images):

PHASE	AREA	PERIMETER (SURFACE)
C_3S	0.6794	0.6037
C_2S	0.1714	0.1997
C_3A	0.0703	0.0942
C_4AF	0.0789	0.1024

Overall phase fractions (average of two images):

PHASE	AREA
C_3S	0.5648
C_2S	0.1427
C_3A	0.0585
C_4AF	0.0655
Gypsum	0.0967
Free lime	0.0108
Alkali sulfates	0.0268
Periclase	0.0310

Gypsum typically added as 6.0% on a volume basis.

Use the back button on your Web browser to return to the cement image.

Figure 7: Description of the quantitative analysis for CCRL cement 135.

Information on CCRL Cement 136

Image and correlation files for:
Cement and Concrete Reference Laboratory (CCRL) Cement 136, a Type I ordinary portland cement with a Blaine fineness of about 390 m^2/kg

Color 2D image in cement136.gif (500X magnification- 256 μm by 200 μm)
Red is C_3S, aqua is C_2S, green is C_3A, yellow is C_4AF, pale green is gypsum, white is free lime, dark blue is potassium sulfate, and magenta is a MgCa phase

Discretized particle size distribution is in cement136.psd

Extracted Correlation files (1 μm/pixel):
cm136r.sil --- C_3S and C_2S
cm136r.c3s --- C_3S
cm136r.c4f --- C_4AF

Phase Fractions for four major clinker phases (average of two images):

PHASE	AREA	PERIMETER (SURFACE)
C_3S	0.6560	0.6138
C_2S	0.1812	0.1766
C_3A	0.0665	0.0906
C_4AF	0.0963	0.1189

Overall phase fractions (average of two images):

PHASE	AREA
C_3S	0.5770
C_2S	0.1593
C_3A	0.0584
C_4AF	0.0846
Gypsum	0.0893
Free lime	0.0125
Alkali sulfates	0.0031
Periclase	0.0113

Gypsum typically added as 6.0% on a volume basis.

Use the back button on your Web browser to return to the cement image.

Figure 8: Description of the quantitative analysis for CCRL cement 136.

2.4 Non-evaporable Water Content Determination

One method of quantifying the degree of hydration of a portland cement is via measurement of its non-evaporable water content, after any hydration time of interest [8]. For the non-evaporable water content determinations, cement pastes were prepared with a water-to-cement ratio (w/c) of 0.4. The cement powder and necessary mass of water were mixed together by kneading by hand in a sealed plastic bag for two to three minutes. Samples were then removed and stored in capped plastic vials. After placing the cement paste sample (typically 10 g to 15 g in mass) in its container, the vials were either capped to maintain sealed curing conditions, or about 1 mL of water was added on top of the cement paste to maintain saturated curing conditions throughout the experiment. The samples were stored at 25 °C until their evaluation. Evaluations were typically made after the following hydration times: 8 h and (1, 3, 7, 14, and 28) d.

After achieving the required age, samples for the determination of non-evaporable water content, w_n, were ground to a powder, using a mortar and a pestle, and flushed with methanol, using a porous ceramic filter and a vacuum, to halt the hydration. The resultant powder was divided approximately in half and placed in two crucibles of known mass, which were left overnight (about 20 h) in an oven at 105 °C. When removed from the oven, the mass of the crucibles and samples were redetermined before placing them in a furnace at 1000 °C for a minimum of 4 h. The non-evaporable water content was calculated as the average difference between the 105 °C and 1000 °C mass measurements for the two crucibles, corrected for the loss on ignition of the cement powder itself, which was assessed in a separate experiment.

To convert the non-evaporable water content measurements to estimated degrees of hydration, α, it was necessary to determine the non-evaporable water content for a fully hydrated sample. Based on the compositions of the two cements [3], values of 0.235 g H_2O/g cement and 0.243 g H_2O/g cement were determined for cements 135 and 136, respectively.

3 CEMHYD3D Results

3.1 Hydration Kinetics

Figures 9 and 10 show the model predictions and experimental results for degree of hydration under saturated and sealed conditions for cements 135 and 136, respectively. In both cases, CEMHYD3D does an excellent job of fitting the experimental data and in matching the observed differences between saturated and sealed curing observed at longer hydration times. Early in the hydration process, excess water is readily available, so that the water lost due to self-desiccation in the sealed specimens does not have a major influence on hydration kinetics. As the specimen ages, the amount of self-desiccated (empty) porosity becomes significant, and the hydration rate of the sealed specimens trails behind those of the corresponding saturated specimens. While not a large difference is observed for the w/c=0.4 samples investigated in this study, for lower w/c ratios (now often being employed in high-performance concretes) sealed conditions can lead to a substantial reduction in the degree of hydration (and the strength) achieved at long hydration times (e.g., > 7 d). For these two cements, the conversion factor between hydration cycles and real time is nearly a constant (0.00030 for cement 135 and 0.00036 for cement 136). These values are in good

agreement with a previously used conversion factor of 0.00030 for cement 133 issued by the CCRL in 1999 [4].

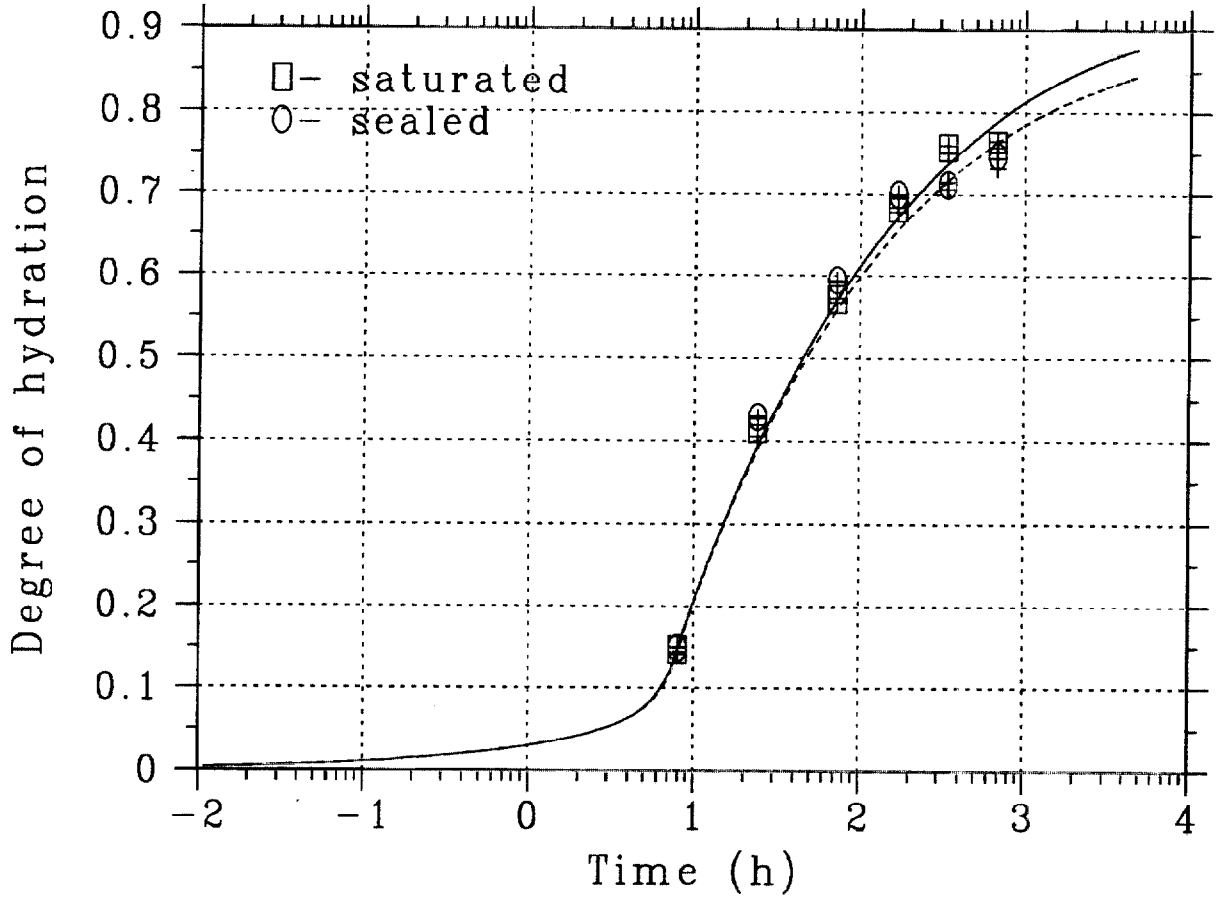

Figure 9: Computer model (lines) and experimental results (data points) for degree of hydration of CCRL cement 135, w/c=0.40, under saturated and sealed curing conditions. Crosses indicate ± one standard deviation in experimental measurements, and generally fall within the boundaries of the data point symbol itself. Model cycle to actual hydration time conversion factor was 0.0003.

3.2 Heat of Hydration

The heat of hydration was determined by the testing laboratories using the ASTM C186 heat of solution test method [1]. For this test, cement pastes with w/c=0.4 were prepared and stored in sealed vials (sealed curing conditions) at 23 °C. At the time of testing, either 7 d or 28 d, the cement paste sample was digested in an acid solution and the energy released measured. By subtracting this measured value from the value determined for the starting cement powder, the heat of hydration may be determined [1]. To predict these values using CEMHYD3D, hydration of a w/c=0.4 cement paste under sealed conditions at 23 °C was conducted for cements 135 and 136. Tables 3 and 4 provide a comparison of the values determined using the standard ASTM C186 method to those predicted by CEMHYD3D. In every case, the CEMHYD3D value is within two standard deviations of the average value determined in the CCRL testing program. It is observed that the CEMHYD3D and ASTM

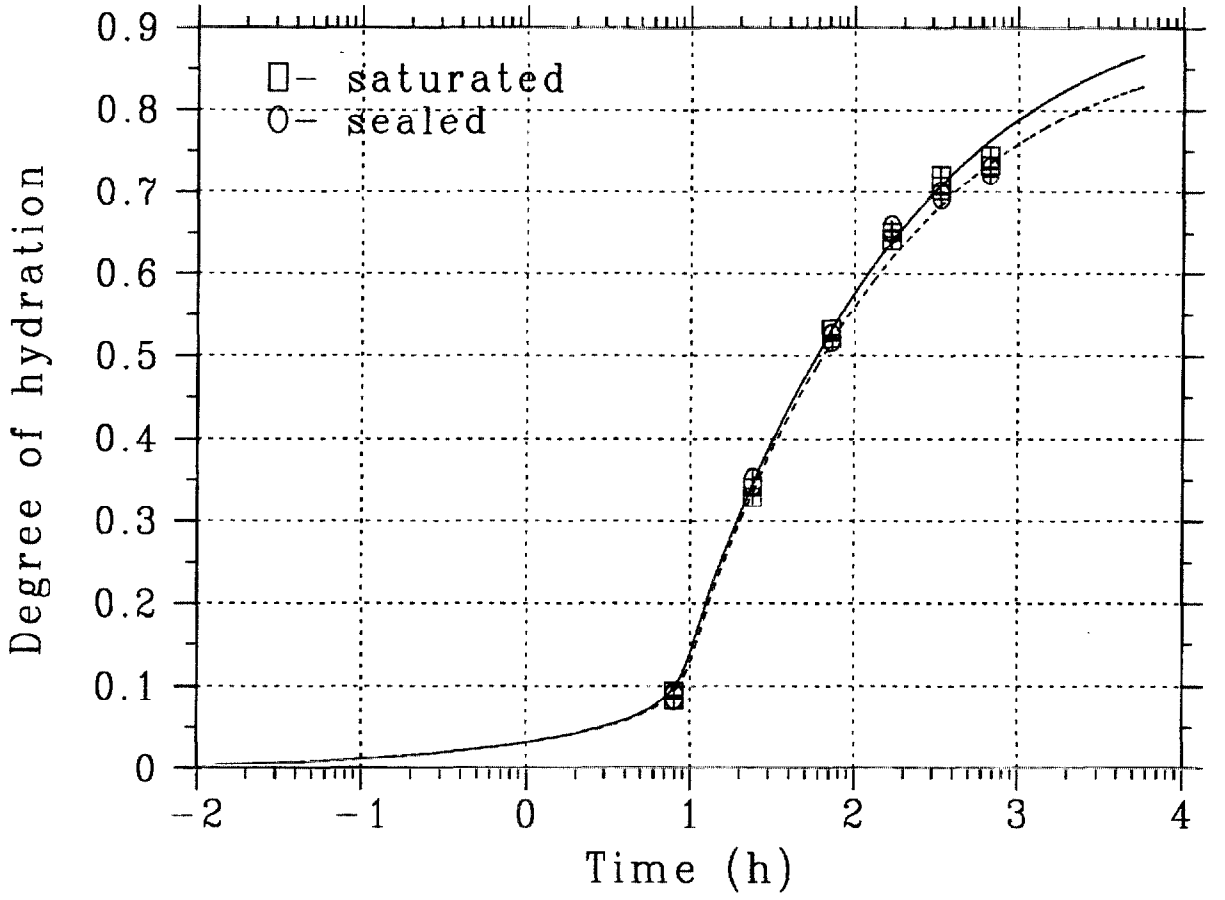

Figure 10: Computer model (lines) and experimental results (data points) for degree of hydration of CCRL cement 136, w/c=0.40, under saturated and sealed curing conditions. Crosses indicate ± one standard deviation in experimental measurements, and generally fall within the boundaries of the data point itself. Model cycle to actual hydration time conversion factor was 0.00036.

C186 values exhibit excellent agreement for the 7 d specimens, with CEMHYD3D slightly overpredicting the measured values at the testing age of 28 d, as it also did for the degree of hydration results presented in Figures 9 and 10.

3.3 Mortar Strength Development

The predicted and measured compressive strength developments are provided in Figures 11 and 12, for cements 135 and 136, respectively. The prefactors used to calibrate to the 3 d measured results were 110.7 MPa and 105.4 MPa for cements 135 and 136, respectively. In the past, calibrating the model to the 3 d measured strength using Powers' gel-space ratio [8] has provided excellent model predictions of 7 d and 28 d measured strengths for CCRL cements 115 and 116 [3] and for CCRL cement 133 [4]. For both cements 135 and 136, however, calibration to the 3 d values resulted in the model overpredicting the 28 d strength. Conversely, calibrating the model values to the 7 d measured strength (using prefactors of 96.5 MPa and 100.3 MPa for cements 135 and 136, respectively) results in model-predicted 28 d values which are within one standard deviation of the measured mean response. The 28 d predictions are still higher than the measured values, in agreement with the observed

Table 3: Heat of Hydration Determinations for Cement 135 (w/c=0.4)

Age	ASTM C186 average (J/g)	ASTM C186 standard deviation	CEMHYD3D prediction (J/g)
7 d	326.4	21.8	338.5
28 d	360.2	19.2	396.0

Table 4: Heat of Hydration Determinations for Cement 136 (w/c=0.4)

Age	ASTM C186 average (J/g)	ASTM C186 standard deviation	CEMHYD3D prediction (J/g)
7 d	318.8	20.5	319.1
28 d	359.4	33.5	381.0

differences in the predicted and measured 28 d heats of hydration provided in Tables 3 and 4. Further research is needed to assess the reliability of the model-predicted strengths for a wider variety of cement types. With this in mind, CCRL cements will continue to be evaluated in this manner as they are released for proficiency analysis in the future.

4 Summary

CCRL Cements 135 and 136 have been quantitatively characterized based on SEM/X-ray imaging. The quantitative phase compositions estimated from the SEM images differ significantly from those computed using the formulas developed by Bogue. Based on the SEM/X-ray analysis, starting three-dimensional cement particle microstructures were created and hydrated using the CEMHYD3D program. Model predictions for degree of hydration, heat of hydration, and mortar strength development were compared to their experimental counterparts, with reasonably good agreement. It is planned to continue to perform the SEM and CEMHYD3D analyses on all future cements issued in the CCRL proficiency sample program and make the SEM results available in the online database available at http://ciks.cbt.nist.gov/phpct/database/images.

5 Acknowledgements

The authors would like to acknowledge the NIST Partnership for High Performance Concrete Technology program for funding this research and Mr. Robin Haupt of the Cement and Concrete Reference Laboratory for supplying the samples of cements 135 and 136.

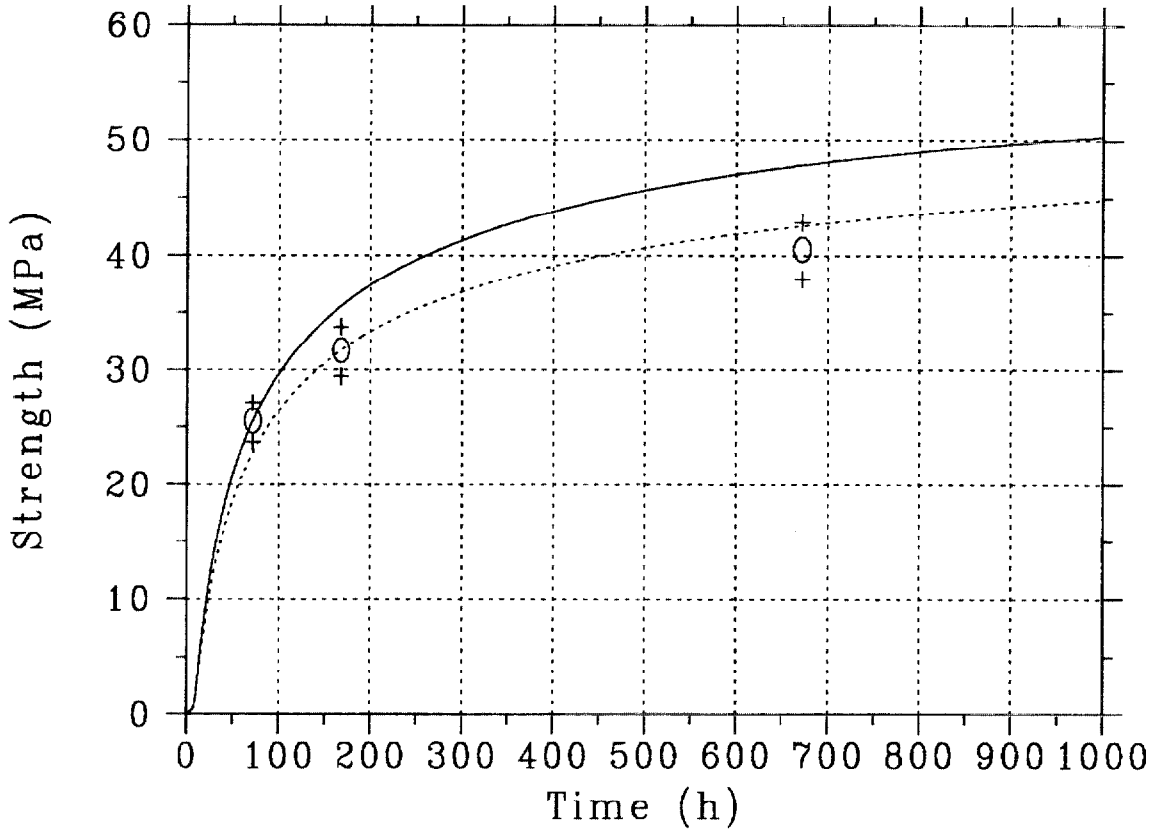

Figure 11: Experimentally measured (circles) and model-predicted compressive strength development for ASTM C109 mortar cubes prepared from CCRL cement 135. Solid line indicates model calibration to the 3 d measured strength while dotted line indicates calibration to the 7 d measured value. Crosses indicate ± one standard deviation from the mean, as determined in the CCRL testing program.

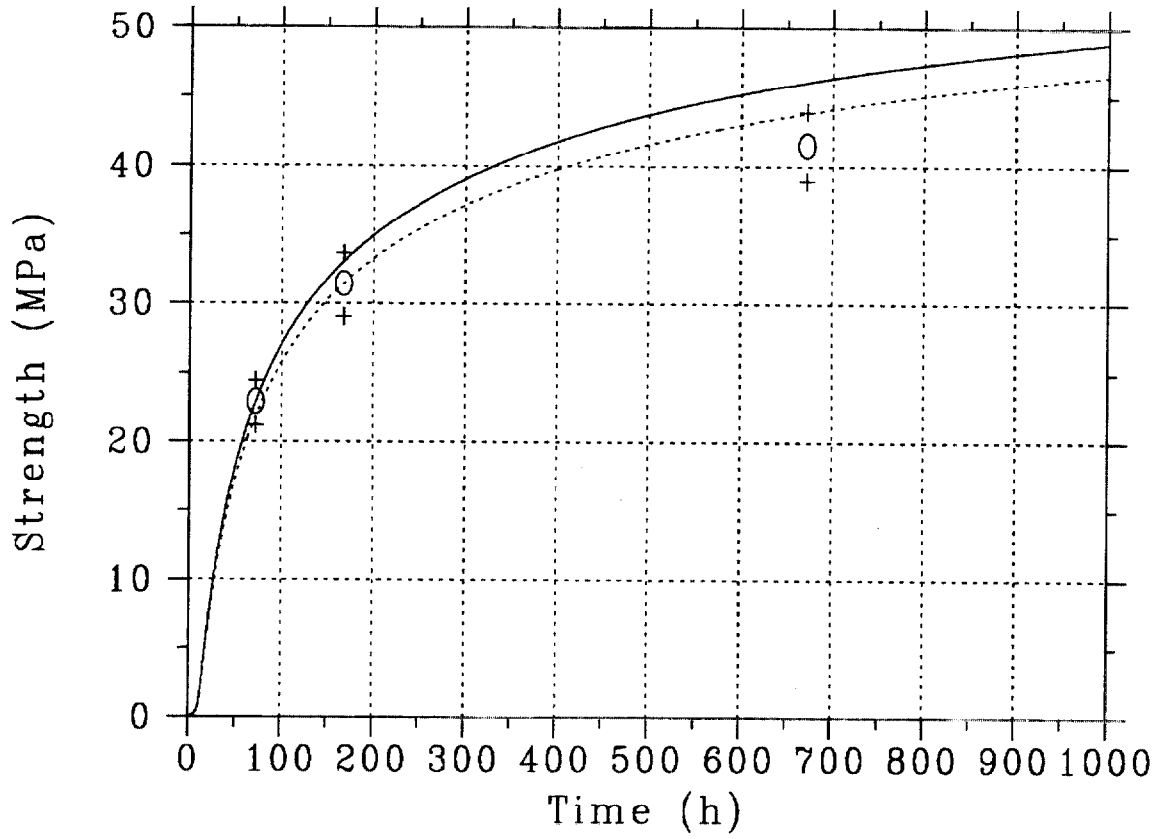

Figure 12: Experimentally measured (circles) and model-predicted compressive strength development for ASTM C109 mortar cubes prepared from CCRL cement 136. Solid line indicates model calibration to the 3 d measured strength while dotted line indicates calibration to the 7 d measured value. Crosses indicate ± one standard deviation from the mean, as determined in the CCRL testing program.

References

[1] ASTM Annual Book of Standards, Vol. 04.01 Cement; Lime; Gypsum (American Society for Testing and Materials, West Conshohocken, PA) 1999.

[2] Cement and Concrete Reference Laboratory Proficiency Sample Program: Final Report on Portland Cement Proficiency Samples Number 135 and Number 136, Cement and Concrete Reference Laboratory, Gaithersburg, MD, March 2000 (unpublished).

[3] Bentz, D.P., "Three-Dimensional Computer Simulation of Portland Cement Hydration and Microstructure Development," *Journal of the American Ceramic Society*, **80** (1), 3-21, 1997.

[4] Bentz, D.P., "CEMHYD3D: A Three-Dimensional Cement Hydration and Microstructure Development Modelling Package. Version 2.0," NISTIR **6485**, U.S. Department of Commerce, April 2000, available online at http://ciks.cbt.nist.gov/bentz/cemhyd3dv20.

[5] Bentz, D.P., and Stutzman, P.E., "SEM Analysis and Computer Modelling of Hydration of Portland Cement Particles," in Petrography of Cementitious Materials, edited by S.M. DeHayes and D. Stark (ASTM, Philadelphia, PA, 1994) p. 60.

[6] Bentz, D.P., Stutzman, P.E., Haecker, C.J., and Remond, S., "SEM/X-ray Imaging of Cement-Based Materials," in Proceedings of the 7th Euroseminar on Microscopy Applied to Building Materials, Eds. H.S. Pietersen, J.A. Larbi, and H.H.A. Janssen, Delft University of Technology, pp. 457-466 (1999), available online at http://ciks.cbt.nist.gov/bentz/eurosem/semcolor.html.

[7] Castleman, K.R., Digital Image Processing (Prentice-Hall, Englewood Cliffs, NJ, 1979).

[8] Taylor, H.F.W., Cement Chemistry (Thomas Telford, London, 1997).